***Abstract*—This paper provides a comprehensive exploration of Heterojunction Bipolar Junction Transistors (HBTs), essential semiconductor devices in modern electronics. The introduction contextualizes the importance of HBTs, specifically within the realm of heterojunction technology. Characteristics of HBTs are scrutinized, highlighting their unique features and advantages in diverse electronic applications.**

The investigation explores the notion of preliminaries within HBTs, shedding light on their crucial role and influence on the overall performance of the transistor. This includes an analysis of how preliminaries affect key operations like signal amplification and modulation.

A thorough analysis of the HBT structure is presented, covering aspects of material composition and layering in heterojunctions. Different modes of operation, including amplification and switching, are scrutinized to underscore the transistor's versatility and efficiency in various electronic circuits.

Additionally, the paper briefly touches upon the practical applications of HBTs across technological domains, showcasing their adaptability and performance advantages. These applications demonstrate the broad significance of HBTs in advancing semiconductor technology and their role in diverse electronic systems.

I. INTRODUCTION

Heterojunction Bipolar Transistors (HBTs) stand as a cornerstone in semiconductor device innovation, harnessing the unique characteristics of heterostructures to redefine electronic functionalities. This introduction sets the stage by discussing the fundamental significance of HBTs, detailing their distinctive structural composition, and highlighting their pivotal role in advancing contemporary electronics. Furthermore, it outlines the sections to follow, offering an overview of the paper's contents, which encompass the theoretical foundations, structural insights, operational principles, practical applications, numerical assessments, and conclusive remarks on HBTs.

II. PRELIMINARIES

The distinctive strength of the Heterojunction Bipolar Transistor (HBT) architecture lies in its utilization of wide-gap emitters, leading to an increased current gain. This arises from the reduced carrier injection from the base into the emitter, attributed to a larger energy barrier in the valence band of emitters (for NPN HBTs) compared to homojunction transistors. As a result, there is no longer a necessity for a doping structure to maintain a specific current gain. The unique characteristic of HBTs, stemming from this flexibility, is their bipolar transistor function.

HBT architectures offer the advantage of achieving lower base resistance and reduced base-emitter capacitance, thereby significantly enhancing high-speed performance and electron transport. The conceptualization of HBTs traces back to Shockley's introduction in 1948, with Kroemer later formulating a theoretical basis for HBTs based on the diffusion model. This has garnered substantial interest in the field of high-speed electronics.

Early attempts to identify potential heterojunctions for emitter-base combinations faced challenges due to difficulties in creating effective heterointerfaces. Heterojunctions composed of Group IV binary or binary-binary materials, such as Ge-GaAs, Ge-ZnSe, and GaAs-ZnSe, encountered limited success, primarily due to the high generation-recombination current resulting from a high deep-level density. The utilization of lattice-matched ternary or quaternary systems, particularly AlGaAs and InGaAsP using liquid-phase epitaxy (LPE), gained traction in manufacturing optoelectronic devices.

The significance of the wide-gap emitter in achieving substantial current increases was demonstrated by HBTs generated from these III-V material systems. In 1975, an AlGaAs-GaAs HBT claimed a current gain of 350. Challenges with HBTs generated by LPE included poor controllability in the layer structure and insufficient thickness uniformity. The advancement of realistic HBTs using the AlGaAs material system was facilitated by novel epitaxial-growth techniques, notably molecular-beam epitaxy (MBE) and metal-organic chemical vapor deposition (MOCVD). These methods excel in creating precise HBT structures, including grading band gaps and obtaining densely doped layers with optimal conductivity.

III. STRUCTURE

A heterojunction bipolar junction transistor (HBT) is a type of bipolar transistor where the junction between different semiconductor materials forms the basis of its operation. **Here's a breakdown of its structure:**

1.Substrate or Base Layer:It begins with a substrate layer, typically made of a semiconductor material like silicon (Si), gallium arsenide (GaAs), or other compound semiconductors. This layer provides a foundation for building subsequent layers.

2.Emitter Layer:Above the substrate layer, there is an emitter layer. This layer consists of a semiconductor material with a different bandgap compared to the substrate. For example, if the substrate is made of GaAs, the emitter might be made of a different semiconductor material like AlGaAs (aluminum gallium arsenide).

3.Base Layer:Between the emitter and the substrate, there's a base layer. This layer is usually very thin and controls the flow of current between the emitter and the collector. The width and composition of this layer significantly affect the transistor's performance.

4.Collector Layer: The layer below the substrate (or sometimes connected to the substrate) is the collector layer. It often shares the same material as the substrate but might have different doping or composition to aid in the transistor's operation.

5.Contacts and Metal Layers: Metal contacts are used to connect to the different layers of the transistor to enable external connections for input (base and emitter) and output (collector). Metal layers are often deposited on top of the semiconductor layers to facilitate these connections.

Remark 1 *The key feature of an HBT is the heterojunction formed between different semiconductor materials. This heterojunction allows for a more efficient operation compared to traditional homojunction bipolar transistors due to the differences in bandgap energies between the layers. This enables better control of the flow of charge carriers and improves the*

transistor's performance in terms of speed, power efficiency, and frequency capabilities.

Remark 2 *HBTs are commonly used in high-frequency applications like telecommunications, satellite communication, and high-speed digital circuits due to their superior performance characteristics compared to standard bipolar junction transistors (BJTs).*

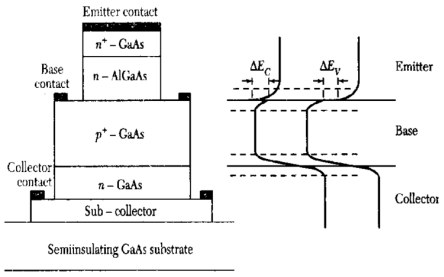

Fig. 1: Structure of HBT

Heterojunction bipolar transistors (HBTs) are devices where different semiconductor materials with different bandgaps are used to form the junctions within the transistor. These heterojunctions allow for enhanced performance compared to conventional bipolar junction transistors (BJTs). The different structures of HBTs significantly impact their performance in terms of speed, power handling, and frequency response. **Here are some different structures of HBTs along with their impacts on performance:**

1.Single Heterojunction Bipolar Transistor (SHBT):

Structure: Consists of one heterojunction between two different semiconductor materials.

Impact: Offers improved current gain, reduced base transit time, and higher frequency operation compared to conventional BJTs due to the heterojunction reducing the charge storage effects.

2.Double Heterojunction Bipolar Transistor (DHBT):

Structure: Contains two heterojunctions, typically with three different semiconductor materials (e.g., emitter, base, and collector).

Impact: Provides even better performance compared to SHBTs by reducing the base-collector capacitance and enhancing charge confinement within the base region, leading to higher speed, lower power consumption, and improved high-frequency response.

3.Graded Heterojunction Bipolar Transistor (GHBT):

Structure: Utilizes a graded composition of semiconductor materials at the heterojunctions, creating a smooth transition in the bandgap.

Impact: Minimizes the discontinuities in the energy band structure, reducing carrier trapping and enhancing electron mobility, thereby improving the device's speed and reducing the frequency limitations caused by bandgap discontinuities.

4.Superlattice Heterojunction Bipolar Transistor (SHBT):

Structure: Employs alternating thin layers of different semiconductor materials to create a superlattice structure at the junctions.

Impact: Enhances carrier transport properties by manipulating the energy band structure, reducing the transit time and enabling high-speed operation at very high frequencies.

Remark 3 *The impact of these structures on HBT performance includes factors such as higher frequency operation, reduced transit times, lower power consumption, improved current gain, and better linearity. However, the fabrication complexity and costs may increase with more advanced structures.*

IV. Operation of a HBT

The HBT works exactly as a BJT. The base-emitter junction is forward biased, and the collector-base junction is reversed biased. The equilibrium is disturbed, and electrons are injected from the emitter into the base. They diffuse across the base until they reach the edge of the base-collector depletion region and are immediately accelerated across the base-collector junction into the collector where they are majority carriers and can contribute to the collector current. The base current is due to the holes diffusing from the base into the emitter and there is also a small contribution from any electrons that fail to make it across the base because they recombine. The ratio of electron current to hole current in the general case where the emitter and base may be made of different semiconductors is:

$$\frac{I_n}{I_p} = \frac{D_n N_D L_p}{D_p N_A W_B} \cdot \left(\frac{{n_{iE}}^2}{{n_{iB}}^2}\right)$$

NA and ND are emitter and base doping, niB2 and niE2 are the electron-hole products for the emitter and base, Dp and Dn are the hole and electron diffusion constants, WB is the base width and Lp the hole diffusion length. For the HBT niB2 and niE2 are no longer the same.

$${n_i}^2 = N_c N_v e^{-\frac{E_g}{k_b T}}$$

$$\frac{I_n}{I_p} \sim \frac{D_n N_D L_p}{D_p N_A W_B} e^{\frac{\Delta E_g}{k_b T}}$$

For sufficiently large δ Eg (δ Eg = 0 for a BJT), Ip will be completely suppressed, virtually independent of either the emitter and base doping or base width. For example, at an Al mole fraction of 30 percent,

$$e^{\frac{\Delta E_g}{k_b T}} \sim 10^6.$$

With this additional factor of 106 (compared to BJT), the device designer may choose doping levels and base width freely in order to optimize other aspects of performance, such as speed.

Heavy doping of the emitter widens the more lightly doped base depletion region, resulting in base width change vs. base-emitter voltage change, which in turn causes base width

modulation, decreased linearity, and in the worst case, punch-through.

In general, the base width is small, and therefore most of the electrons travel through the base due to their momentum and are collected by the collector. However, a small number of electrons are lost due to recombination in the emitter-base depletion region and in the base region.

V. Characteristics

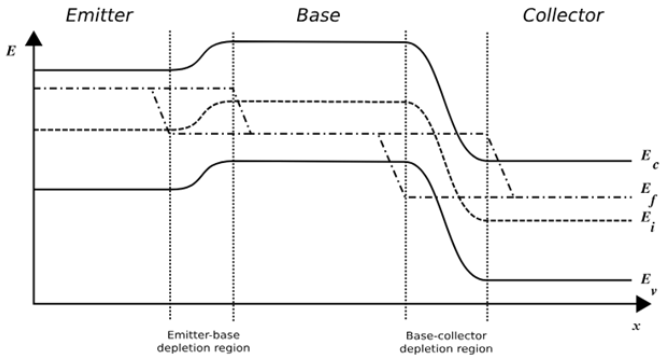

Fig. 2

$$n_B = n_{B0}\left[\exp\left(\frac{qV_{BE}}{kT}\right)-1\right] = \frac{n_{i2}^2}{P_B}\left[\exp\left(\frac{qV_{BE}}{kT}\right)-1\right]$$
$$= N_{c2}\exp\left[\frac{-(E_{g2}+\Delta F_2)}{kT}\right]\left[\exp\left(\frac{qV_{BE}}{kT}\right)-1\right]$$

Fig. 3

$$P_E = P_{E0}\left[\exp\left(\frac{qV_{BE}}{kT}\right)-1\right] = \frac{N_{i1}^2}{N_E}\left[\exp\left(\frac{qV_{BE}}{kT}\right)-1\right]$$
$$= N_{v1}\exp\left[\frac{-(E_{g1}+\Delta F_1)}{kT}\right]\left[\exp\left(\frac{qV_{BE}}{kT}\right)-1\right].$$

Fig. 4

$$I_E = \mathrm{Sq}\left(\frac{D_B}{L_B}\right)n_{B0}\coth\left(\frac{W_B}{L_B}\right)\left[\left\{\exp\left(\frac{qV_{BE}}{kT}\right)-1\right\}-\frac{1}{\cosh\left(\frac{W_B}{L_B}\right)}\left\{\exp\left(\frac{qV_{BC}}{kT}\right)-1\right\}\right]$$

$$+ Sq\left(\frac{D_E}{L_E}\right)P_{E0}\left\{\exp\left(\frac{qV_{BE}}{kT}\right)-1\right\}.$$

Fig. 5

$$I_E = \mathrm{Sq}\left[\left(\frac{D_B}{L_B}\right)n_{B0}\coth\left(\frac{W_B}{L_B}\right)+\left(\frac{D_E}{L_E}\right)P_{E0}\right]\exp\left(\frac{qV_{BE}}{kT}\right),$$

Fig. 6

$$I_C = \mathrm{Sq}\left(\frac{D_B}{L_B}\right)n_{B0}\frac{1}{\sinh\left(\frac{W_B}{L_B}\right)}\left[\left\{\exp\left(\frac{qV_{BE}}{kT}\right)-1\right\}\right.$$
$$\left.-\coth\left(\frac{W_B}{L_B}\right)\left\{\exp\left(\frac{qV_{BC}}{kT}\right)-1\right\}\right]-\mathrm{Sq}\left(\frac{D_C}{L_C}\right)P_{C0}\left\{\exp\left(\frac{qV_{BC}}{kT}\right)-1\right\}.$$

Fig. 7

$$I_C = \mathrm{Sq}\left(\frac{D_B}{L_B}\right)n_{B0}\sinh^{-1}\left(\frac{W_B}{L_B}\right)\exp\left(\frac{qV_{BE}}{kT}\right).$$

Fig. 8

$$I_B = \mathrm{Sq}\left(\frac{D_B}{L_B}\right)n_{B0}\left[\coth\left(\frac{W_B}{L_B}\right)-\sinh^{-1}\left(\frac{W_B}{L_B}\right)\right]\exp\left(\frac{qV_{BE}}{kT}\right).$$

Fig. 9

$$h_{fe} = \frac{\Delta I_C}{\Delta I_B} = \frac{1}{\cosh(W_B/L_B)-1} \sim 2\left(\frac{L_B}{W_B}\right)^2.$$

Fig. 10

With the exception of employing a wide-gap emitter, the output current regulation mechanism in an Heterojunction Bipolar Transistor (HBT) closely mirrors that of a homojunction bipolar transistor. The primary regulation of electron injection current stems from the conduction band in the base. Illustrated in Figure 3, a typical NPN HBT band diagram reveals that the barrier for holes is greater than that for electrons due to distinct band-gap energies in the base and emitter regions. A reduced hole population on the valence band of the emitter layer leads to a lower hole injection current, consequently enhancing emitter injection efficiency and increasing current gain.

In the depicted Figure 3 , a graded emitter refers to a configuration where the band-gap energy at the emitter-base junction continuously adjusts. In such cases, the flow of injection current is primarily governed by the diffusion of minority carriers, especially when the emitter is graded, resulting in a uniform base layer and smooth fluctuations in the quasi-Fermi level. The formulation of homojunction Bipolar Transistors (BTs) based on the diffusion model can be classically established in this context. For more detailed insights, you can refer to S. M.

Sze's "Physics of Semiconductor Devices," 2nd ed., Chapter 3, published by Wiley in 1981.

In the context of a one-dimensional NPN HBT, certain key expressions are presented, with a focus on simplicity by disregarding the generation-recombination current at the emitter-base depletion layer. The minority carrier densities on the base side (n8) and the emitter side (PE) at a base-emitter voltage (V8E) are identified at each depletion layer edge. It's important to note that the equilibrium minority carrier densities n80 and PEO undergo exponential changes with band-gap energy. In cases where a wide-gap emitter is employed (Eg1 $\rangle\rangle$ Eg2), PEO can be significantly reduced compared to n80, as evident from equations in fig (3) and (4). Similar boundary constraints for minority carriers akin to homojunctions exist in this scenario.

The first term in equation in fig (5) addresses the electron diffusion current within an emitter distinguished by an infinitely thick neutral-base layer denoted as W8. The subsequent part accounts for the hole diffusion current. The overall collector current (Ic) is computed using the calculation specified in the equation.

In equation in fig(5), the initial segment denotes the electron diffusion current linked to an emitter characterized by an infinitely thick neutral-base layer, identified as W8. The following aspect corresponds to the hole diffusion current. The resultant collector current (Ic) is established by the equation IB = IE – IC. It is important to note that the introduction of minority carriers at the base-collector junction is minimal within the active zone of the transistor.

By employing a wide-gap emitter, the second term in equation in fig (7) can be significantly diminished to an extremely low level. This situation allows for some flexibility in determining the base and emitter dopings. In the case of AlGaAs-GaAs HBTs, the base doping levels are typically targeted in the range of $10^{19}\ cm^{-3}$, surpassing those of Si BTS by more than an order of magnitude. HBTs may feature an emitter doping as low as approximately $10^{17}\ cm^{-3}$, resulting in a reduced emitter capacitance. The decrease in emitter capacitance during operation is also attributed to an elevation in the inherent voltage of the emitter-base junction due to a conduction-band discontinuity. The estimation of IB is derived by disregarding the hole diffusion current in equation in fig(7).

The current gain (hfe) in an HBT, illustrated in Figure (10), represents the ratio of collector current to base current, indicating the transistor's amplification capability. A high hfe value signifies efficient current amplification, crucial for HBT performance.

The importance of maintaining a high current gain in HBTs is underscored by the critical role of the diffusion length in the base, denoted as$LB(te * DB)^{0.5}$. This expression highlights the significance of LB in preserving a robust current gain. Additionally, the density of base doping and nonradiative recombination center density significantly influences the minority carrier lifespan τe.

VI. APPLICATIONS

A. optoelectronic mixer (OEM in ROF system) Radio over fiber (RoF) machine is the solution for the imparting incredibly reliable verbal exchange service. This machine is characterized via having both a fiber optic hyperlink and loose-space radio path to exploit the synergy of two complementary technology; the broadband mobile wi-fi get right of entry to and stuck optical get admission to. Optoelectronic blending is required in RoF structures to hit upon the RF modulated optical signal and carry out frequency up-conversion. On this work, 3-terminal InP/InGaAs HBT with optical get admission to has been used because the optoelectronic mixer (OEM) for the front-quit RoF optical receiver configuration. Consequently on this configuration, the photodetection and frequency conversion may be carried out in p-i-n photodiode and HBT tool, which extensively simplify the traditional technique. HBT has been recognized as a suitable tool to be applied in optoelectronic mixers through simultaneously photodetecting an depth modulated laser beam at 1550nm and frequency translating the detected signal to a higher or decrease frequency which can offer excessive mixing efficiency and required situation for an oscillator. The HBT OEM was designed, modeled and simulated by using the usage of APSYS Crosslight software. Records from the simulation together with the gummel plot, energy band diagram and other characteristics had been generated and analyzed. The device changed into analyzed considering 1550nm wavelength with as much as 30GHz modulating signal frequency. As a result, the designed HBT is discovered to be feasible for the implementation of the broadband RoF machine as it may carry out the photodetection, amplification and frequency conversion simultaneously as required at RoF far flung antenna unit. The RoF OEM changed into effectively simulated using a nonlinear microwave simulator to carry out harmonics balance evaluation, which represented real photodetection model and nonlinear dynamic optoelectronic blending conduct. On this paper we suggested the - 5.2 dB most internal blending efficiency for four hundred MHz IF modulated sign to 3.4 GHz upconverted RF sign with LO electricity is -2dBm, and that agreed with conventional theoretical analysis.

B. InP HBT IC Distinctly scaled indium phosphide (InP) heterojunction bipolar transistor (HBT) technologies were tested with most frequencies of oscillation (f max) of $\rangle$ 1 THz and circuit operation has been extended into the decrease end of the terahertz (THz) frequency band. InP HBT technologies are considered as ultra-excessive-performance energy amplifiers as they offer excessive radio-frequency (RF) output electricity density, millivolt (mV) threshold uniformity, and excessive stages of integration. Integration with multilevel thin-film wiring permits the realization of compact and complicated THz monolithic included circuits (TMICs). Circuit effects suggested from InP HBT technologies encompass: two hundred-mW strength amplifiers at 210 GHz, 670-GHz amplifiers and essential oscillators, and fully integrated six hundred-GHz transmitter circuits. We review the country of the artwork in THz-capable InP HBT devices and integrated circuit (IC) technologies. Understanding ultra-high-efficiency energy amplifiers working at five.Eight GHz is a key problem for wireless strength transmission together with space sun-electricity satellite systems and wi-fi smart-grid quick-distance electricity supply structures. To achieve extremely-

high efficiency, modern-day and voltage waveform control is quintessential to dispose of electricity dissipations at the harmonic frequencies and to preserve a balance between the furnished DC energy and the five.Eight-GHz output electricity. InP heterojunction bipolar transistors (HBTs) with THz-class transistor bandwidth show PAs with excessive RF electricity density and high efficiency at frequencies between one hundred-300GHz. We evaluate the performance of a latest InP HBT IC generation and pronounced IC (HBT IC) outcomes which are applicable to destiny sub-THz communications systems. We have presented a high overall performance 0.25 um InP HBT IC generation with an extrapolated electricity gain cutoff frequency of 1THz. The generation is appropriate for IC demonstrations on the lower quit of the THz frequency band. The initial demonstration of key circuit building blocks provided suggests the era gives a promising path for developing absolutely incorporated THz transceivers. Future work is targeted on the improvement of a 130nm HBT technology for operation at even higher frequencies.

C. High-Voltage GaAs Power-HBTs for Base-Station Amplifiers

HBTS with excessive breakdown voltage for excessive-voltage operation have been evolved, which display exceptional energy skills. Fairly small 10-finger devices of 10x3x30 pm emitter length could be operated adequately at 27 V collector-emitter bias on un-thinned wafer with out warmth sinking. They supply three.2 W of microwave power with a PAE of 74Base stations for second and 0.33-technology cellular networks require high-strength amplifiers. GaAs hetero bipolar transistors (HBTs) provide each excessive power-introduced performance (PAE) and properly linearity. Therefore, they're increasingly more used in cell-handset electricity degrees in the 2 GHz frequency range. An average utility is the 3V, 1W unit mobile. The situation in base stations is distinct due to the fact better energy is required but, then again, larger bias voltages are to be had. The new UMTS networks call for for extraordinarily linear electricity amplifiers, which in turn drives power levels up taking gain of lower back-off operation. So What one needs is a tool unit mobile turning in approximately 10 W at 27 V bias voltage. Furthermore, the ensuing output impedance needs to be large enough to allow for parallel Operation of numerous cells without degrading combining efficiency.

VII. Numerical Evaluation

Experiment and analysis The InGaP/GaAs SHBTs used in this study are commercial products from WIN Semiconductors Corp. The device structure is very similar to that of a conventional AlGaAs/GaAs SHBTs except the AlGaAs emitter layer replaced by an InGaP layer. In the InGaP/GaAs SHBTs, the base–emitter is a heterojunction and the device is passivated with SiN.

Modeled results and discussions Extraction of the forward Gummel current parameters is as follows. The IBEN and NEN can be determined from the intercept and the slope of log(IBE)–VBE plot in the region of low VBE, and then the values of IBEI and NEI are easily obtained by fitting the log(IBE)–VBE curve in the high injection region. The IS and NF are found the same way from the measurement of ICC. For extraction of the reverse Gummel current parameters, similar method with the forward parameter extraction, IBCI, IBCN, NCI and N

Numerical Simulation of Self-heating InGaP/GaAs HBTs

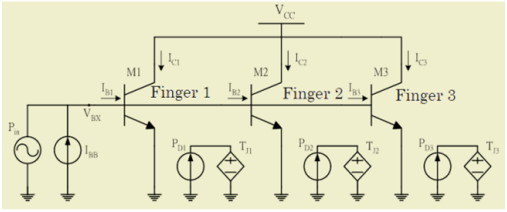

Fig. 11: Model of HBT

(WR), the monotone iterative (MI), and Runge-Kutta methods, a set of nonlinear ordinary differential equations (ODEs) with thermal models is solved numerically in the time domain. The governing ODEs of the equivalent circuit of HBTs are formulated by the Kirchhoff's current law . This solution technique has recently been developed by us for circuit simulations. The temperature-dependent physical quantities are modeled and several important engineering factors, such as the power-added efficiency and the 1-dB compression point of the simulated three-finger HBT are calculated. Our modeling and simulation successfully explores the self-heating and the thermal coupling phenomena of the studied three-finger transistors circuit operated under high power and high frequency conditions.

Self-heating Modeling and Numerical Method

A multifinger HBT is formed by several sub-HBTs with their own collector and emitter, where their base is connected together. As shown in Fig. 11, an equivalent circuit with a thermal network of the three-finger HBT is studied in this work, where each finger is theoretically assumed to be identical. A thermal model that describes the relation between the power dissipation and the junction temperature is adopted. The electrical model of HBT considered in our simulation is based on the Gummel-Poon (GP) large signal model . For the thermal-electrical feedback mechanism, the temperature-dependant equations are introduced to the GP model

$$E_g(T_J) = E_g(T_A) + \frac{E_a \cdot T_A^2}{T_A + E_b} + \frac{E_a \cdot T_J^2}{T_J + E_b} \quad ,$$

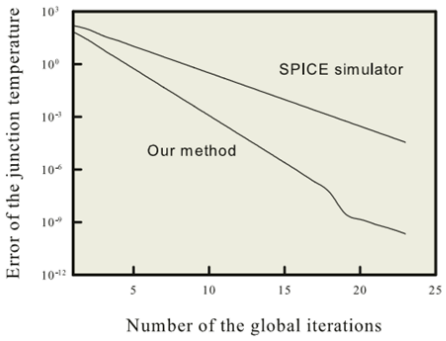

Fig. 12

A plot of the maximum norm error of the junction temperature versus the number of iterations of the WR loop.

$$IS(T_J) = IS \cdot (\frac{T_J}{T_A})^{XTI} \cdot exp[(\frac{E_g(T_A)}{k \cdot T_A}) - (\frac{E_g(T_J)}{k \cdot T_J})],$$

$$ISE(T_J) = ISE \cdot (\frac{T_J}{T_A})^{\frac{XTI}{NE} - XTB} \cdot exp[(\frac{E_g(T_A)}{NE \cdot k \cdot T_A}) - (\frac{E_g(T_J)}{NE \cdot k \cdot T_J})],$$

$$ISC(T_J) = ISC \cdot (\frac{T_J}{T_A})^{\frac{XTI}{NC} - XTB} \cdot exp[(\frac{E_g(T_A)}{NC \cdot k \cdot T_A}) - (\frac{E_g(T_J)}{NC \cdot k \cdot T_J})],$$

$$BF(T_J) = BF \cdot (\frac{T_J}{T_A})^{XTB},$$

$$BR(T_J) = BR \cdot (\frac{T_J}{T_A})^{XTB},$$

where TJ and TA are the junction and the ambient temperature, respectively. We note that for high power devices, TA is the temperature on the back of the substrate. Above equations include the temperature dependance of energy band gap (Eg), the saturation current (IS), the collector and emitter leakage current (ISC and ISE), and the current gain (BF and BR). The thermal model expresses the relation between the power dissipation and the junction temperature. The junction temperature with considering the temperature-dependent thermal conductivity for the three-finger HBT is given by Numerical Simulation of Self-heating InGaP/GaAs.

Relation between V(ce) and I(cc)

The testing case is the device with the collector voltage VCC = 5V , the input current bias IBB = 0.5mA, the frequency is centralized at 1.8GHz, and the convergence criterion is that the maximum norm error of the output voltage is less than 10-11V . Figure 12 shows a plot of the maximum norm error of the junction temperature versus the number of iterations. Simulation with our method demonstrates better convergence property than the result of the SPICE circuit simulator. However, the simulation with the SPICE circuit simulator takes more than 100 iterations to meet the specified stopping criterion. For each time step, the CPU time of our method is of the order of 102 sec. running on a HP workstation XW 8000. The convergence of SPICE circuit simulator depends upon the selection of initial guess and the time steps which complicates the solution procedure for practical engineering application. Our solution algorithm converges monotonically and the DC solutions, in general, are used as the starting solution

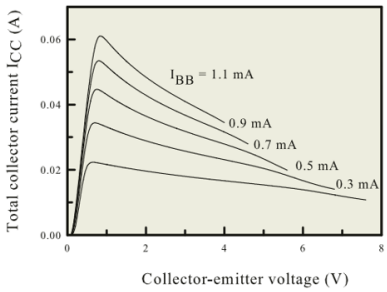

Fig. 13

Conclusion is that The curves of ICC -VCE with respect to different IBB for the simulated three finger InGaP/GaAs HBT circuit. It is significantly different from the result without considering the self-heating.

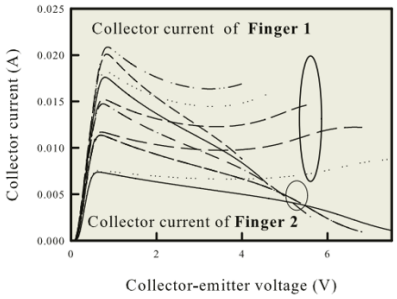

Fig. 14

The simulated ICC -VCE curves with respect to different IBB for the fingers 1 and 2 of the HBT. The result of Finger 3 is omitted according to the property of symmetry The simulated I-V characteristics of the three-finger InGaP/GaAs HBT circuit are shown in Figs.

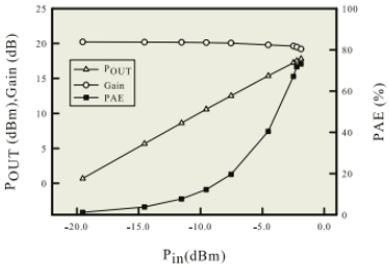

Fig. 15

collector current under constant IBB. Due to the effect of self-heating, the total collector current decreases when the collector-emitter voltage increases, shown in Fig. 13. It results in a negative differential resistance region in the I-V characteristics and a collapse of current gain in the three-finger

HBT circuit. As shown in Fig. 14, the collector current of the central finger (Finger 2) decreases rapidly, compared with the results of neighbor figures, such as Finger 1. It is due to the strongly coupled heat from its neighbor two fingers, Finger 1 and Finger 3. As the collector-emitter voltage increases even more (VCC $\rangle$ 4V), an abrupt reduction of the collector current of Finger 2 occurs. With the electrical and thermal interaction, our modeling and simulation can explore the phenomenon of collapse for the multifinger HBTs under high voltage and high current bias. As shown in Fig. 15, it is the calculated output power (POUT), the power-added efficiency (PAE), and the power gain (Gain) versus the different values of the input power (Pin). The input excitation is a single tone signal at 1.8 GHz. The bias condition of this single tone simulation is with VCC = 3.6 V and IBB = 0.6 mA. In this simulation, we have taken the effect of heating of the input high frequency signal into consideration. It is found that, shown in Fig. 15, the Gain and PAE degrade as Pin increases, and the 1 - dB compression point (P1-dB) is -2.45 dBm. The effect of thermal coupling among fingers also influences the performance of the three-finger device structure. the PAE of the central finger (Finger 2) is reduced and degraded when Pin$\rangle$ -3dBm. In the meanwhile, the PAE of the neighbor finger (Finger 1) still increases as Pin increases. This phenomenon illustrates that the performance degradation of the whole transistor is mainly dominated by the hotter central finger

VIII. CONCLUSION

In conclusion, this paper has provided a comprehensive journey through the realm of Heterojunction Bipolar Transistors (HBTs), elucidating their structural intricacies, operational principles, and practical significance in electronic systems. The exploration of theoretical underpinnings, numerical evaluations, and practical applications underscores the unparalleled potential of HBTs in high-performance electronics. With their unique heterostructure design and remarkable characteristics, HBTs continue to be instrumental in shaping the landscape of modern technology, promising further advancements and innovations in electronic devices and systems. The study underscores the crucial importance of HBTs in driving technological progress and their continued relevance in the ever-evolving field of semiconductor devices.

IX. REFRENCES

we use

1) First reference
2) second reference
3) third reference
4) forth reference
5) fifth reference
6) sixth reference
7) seventh reference
8) 8^{th} reference
9) 9^{th} reference